Paper III

K. M. Laundal, N. Østgaard, K. Snekvik and H. U. Frey (2010)

Inter-hemispheric observations of emerging polar cap asymmetries

Journal of Geophysical Research Vol. 115, doi:10.1029/2009JA015160

III

JOURNAL OF GEOPHYSICAL RESEARCH, VOL. 115, A07230, doi:10.1029/2009JA015160, 2010

Interhemispheric observations of emerging polar cap asymmetries

K. M. Laundal,[1] N. Østgaard,[1] K. Snekvik,[2] and H. U. Frey[3]

Received 3 December 2009; revised 2 March 2010; accepted 1 April 2010; published 30 July 2010.

[1] In this paper we use simultaneous global UV images of the aurora in the two hemispheres to study differences in the polar cap boundary location. We show that the northern and southern auroral ovals circumvent the same amount of magnetic flux, providing additional evidence that the poleward boundary of the aurora coincides with the open/closed field line boundary. During a period of significant flux closure, large asymmetries in the polar cap boundaries developed between the hemispheres. The asymmetry was strongest in the regions where the polar caps contracted the most, suggesting that emerging interhemispheric polar cap asymmetries is an intrinsic phenomenon during substorm expansions, when magnetic flux closes rapidly in the tail. Utilizing the prolonged surveillance of the open/closed boundary location, we show that the growing asymmetries can be accounted for by differences in the ionospheric convection in the two hemispheres. The observations suggest that the differences in convection were due to seasonal differences between the hemispheres, and that the summer hemisphere responded more promptly to changes in magnetospheric convection than the winter hemisphere.

Citation: Laundal, K. M., N. Østgaard, K. Snekvik, and H. U. Frey (2010), Interhemispheric observations of emerging polar cap asymmetries, *J. Geophys. Res.*, *115*, A07230, doi:10.1029/2009JA015160.

1. Introduction

[2] The Earth's magnetosphere is the cavity in space which is dominated by the magnetic field generated in the planet's interior. Its shape differs from a dipole-like field most notably by a long tail which extends to $>100R_E$ (Earth radii) on the nightside of the Earth. This tail is the product of interaction with the interplanetary magnetic field (IMF), which is transported from the sun by the solar wind plasma. When the IMF and the Earth's field have opposite orientations, the field lines can merge on the dayside in a process called reconnection, and form open field lines. Open field lines are then transported, by the influence of the solar wind momentum, anti-sunward, and add to the tail on the nightside. When open field lines with foot-points in opposite hemispheres meet in the tail, they can reconnect, forming a closed field line. Owing to the stretched character of the newly closed field lines, the plasma now convects back to the dayside where it can once again merge with the IMF. This so-called Dungey cycle [*Dungey*, 1961] thus describes the circulation of plasma within the magnetosphere.

[3] The regions at the surface of the Earth which are threaded by open field lines are called the polar cap. The polar caps are very often seen to be encircled by a belt of precipitating particles (~keV), which ionize and excite atmospheric constituents to form the aurora borealis and aurora australis. Global auroral images can therefore be used to observe the shape and size of the polar caps, since it can be identified as the dim region surrounded by the bright aurora (the main exception to this is the polar cusp aurora which is located on open field lines, and the theta aurora). This technique has been substantiated [*Carbary et al.*, 2003; *Boakes et al.*, 2008] and utilized extensively in recent years [*Brittnacher et al.*, 1999; *Mende et al.*, 2003a, 2003b; *Milan et al.*, 2003, 2007, 2008, 2009; *Lam et al.*, 2006; *Hubert et al.*, 2006, 2008; *Boakes et al.*, 2009].

[4] Among the main findings established by these studies are that the polar cap expansion (dayside reconnection) and contraction (nightside reconnection) are quasi-uncoupled. The expansion of the polar cap happens mainly when the IMF has a southward component ($B_z < 0$ nT), whereas the contraction of the oval can happen almost explosively during the expansion phase of a substorm [e.g., *Milan et al.*, 2007]. A substorm expansion can be recognized in global auroral images by a sudden local brightening in auroral luminosity, followed by a rapid azimuthal and latitudinal expansion, lasting typically for a few tens of minutes. The quasi-uncoupled dayside and nightside reconnection is called the expanding/contracting polar cap paradigm, and was first suggested by *Siscoe and Huang* [1985], and expanded upon by, e.g., *Lockwood et al.* [1990] and *Cowley and Lockwood* [1992].

[5] The observational studies of the polar cap boundary cited above all focus on one hemisphere. The implicit assumption is that, when an appropriate magnetic coordinate

[1]Department of Physics and Technology, University of Bergen, Bergen, Norway.
[2]Finnish Meteorological Institute, Helsinki, Finland.
[3]Space Sciences Laboratory, University of California, Berkeley, California, USA.

0148-0227/10/2009JA015160

system is used (the two systems which are most-often used are AACGM and, as in the present study, Apex [*Richmond*, 1995], which are similarly defined), the polar caps in the two hemispheres are approximately similar. This assumption is largely necessitated by the lack of simultaneous measurements from both hemispheres. The assumption is certainly true for the total magnetic flux content, but the open/closed field line boundaries are not necessarily identical. Conjugate observations of the local auroral brightening at substorm onset have shown that large spatial deviations (tens of degrees in longitude) may happen, evidencing a temporary asymmetry in the field line about the equatorial plane [*Østgaard et al.*, 2004, 2005b]. *Stubbs et al.* [2005] also employed simultaneous UV images to find that the entire polar caps can be displaced from each other. The displacement seen in these studies was consistent with distorted magnetic field lines, the distortion being in the same direction as the IMF (in particular the y component). Statistical studies of the substorm onset location in relation to the IMF have confirmed these findings [*Liou et al.*, 2001; *Østgaard et al.*, 2007]. The IMF dependent perturbation in the magnetic field has also been demonstrated directly by in-situ measurements [e.g., *Wing et al.*, 1995]. Conjugate studies have also been undertaken, using all-sky cameras on the ground [e.g., *Sato et al.*, 2005] or on air-planes [*Stenbaek-Nielsen and Otto*, 1997, and references therein], and a combination of observations from ground and space [*Frey et al.*, 1999; *Vorobyev et al.*, 2001]. *Vorobyev et al.* [2001] focused on the poleward boundary of the nightside aurora, which they found to be displaced poleward in the Northern (Southern) Hemisphere compared to the Southern (Northern) Hemisphere when the IMF orientation was in the Parker spiral sector $B_x < 0$, $B_y > 0$ ($B_x > 0$, $B_y < 0$).

[6] In the present paper, we take advantage of two fortuitous constellations of the IMAGE and Polar satellites, both equipped with UV imagers, enabling simultaneous observations of the aurora in the Northern and Southern Hemispheres. The main focus is on a strong substorm occurring on 12 May 2001. In this event, we observe highly variable interhemispheric asymmetries in the polar caps, arising in conjunction with significant flux closure.

[7] The method which we employ is described in the next section. In section 3 we present the observations. The findings are discussed in section 4. Section 5 concludes the paper.

2. Method

[8] The IMAGE satellite [*Burch*, 2000] was launched on 25 March 2000 into an elliptical orbit, which after one year in operation had its apogee (~$7R_E$) over the north pole. The FUV instrument on this satellite included three imagers: The Wideband Imaging Camera (WIC), and two Spectropgrahic Imagers, SI-12 and SI-13. Due to their higher sensitivity and spatial resolution, we use WIC images in this study. WIC [*Mende et al.*, 2000] provided images in the LBH wavelength band (140–190 nm). Being mounted on the spinning satellite, and viewing radially outward, it produced images every 123 seconds (the satellite spin period), and had 10 seconds integration time.

[9] The Polar satellite was launched on 24 February 1996. In 2001, precession of its elliptical orbit had enabled prolonged observation of the Southern Hemisphere. In the present study we use the VIS Earth camera [*Frank et al.*, 1995], which observed UV emissions in the wavelength range of 124–149 nm. VIS Earth was mounted on a despun platform, and in the images used here the integration time was 32.5 s, with a nominal cadence of 54 s.

[10] The intensity observed by VIS Earth is dominated by the OI line at 130.4 nm (83% during quiet conditions according to *Frank and Sigwarth* [2003]). Most of the remaining signal stems from the OI emission at 135.6 nm and from the LBH band. Since WIC is only marginally sensitive to the OI lines, some differences are expected in the response of the two cameras to similar auroral features. However, as long as the two cameras observe a prominent poleward boundary in the aurora, these differences will not affect the result in the present study, even if the absolute intensities may differ.

[11] To calculate the polar cap flux content, an accurate determination of the poleward boundary of the aurora is needed at all local times, since this boundary is a proxy for the open/closed field line boundary (OCB). Earlier studies have used an automated routine for this purpose. Possible methods include a functional fit (a gaussian is often used), or a threshold intensity, often accompanied by automatic tests of how well these methods work. In regions where no valid boundary is obtained, interpolation is necessary, if the total magnetic flux content in the polar cap is to be calculated.

[12] Having experimented with various automated routines for determining the boundary, we did not find any single method which worked well in both hemispheres. This is likely because WIC and VIS Earth have significantly different count rates and signal to noise ratios. In the May 2001 event, additional complications arose from dayglow contamination in the northern images. The dayglow was removed using a functional fit to the background counts, but residual Poisson noise was still evident on the dayside part of the image. In many cases, automatic methods also tend to fail in regions where manual inspection clearly shows that a boundary between the background and auroral luminosity is well defined. Since the comparison between the cameras should be based on a common method, we therefore determined the boundaries by eye. This was done by separating the image into 1 hour wide MLT sectors, and plotting the intensity as a function of latitude. The boundary was placed where the intensity profile transition from background to aurora.

[13] Figure 1a shows this method applied on a best case scenario (solid) and a worst case scenario (dotted-dashed). These intensity profiles are from 20 to 21 MLT and 11 to 12 MLT in the WIC image taken 21:26:58 (Figure 3a). On the night side, the boundary can be determined accurately, because of the sharp transition from aurora to background seen at 71°. For the dayside intensity profile, an accurate determination is impossible, neither by eye, nor by any automatic method that we are aware of. These kinds of boundaries were therefore determined by looking at neighboring regions, assuming the OCB to be fairly uniform, or by looking at later images in which the dayside aurora could be recognized, assuming the boundary not to vary much in time. The latter assumption is justified at the dayside by the concurrent stable solar wind and IMF conditions. The two hemispheres were considered independently. All manually

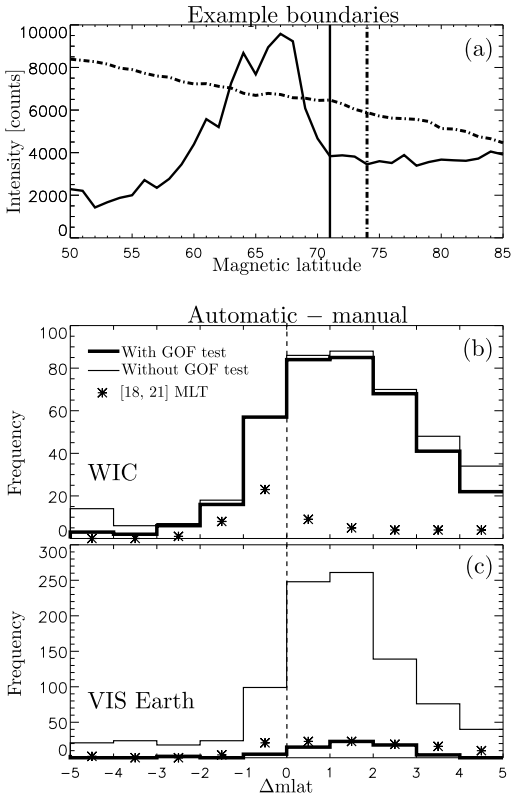

Figure 1. (a) Example of manual boundary determination applied on two intensity profiles, from the WIC image at 21:26:58 UT, 12 May 2001 (Figure 3a). The intensity profiles are from 20–21 MLT (solid) and 11–12 MLT (dotted-dashed). (b and c) The difference (Δ mlat in degrees) between boundaries determined by gaussian fit [*Carbary et al.*, 2003], and our manually determined boundaries, in WIC (Figure 1b) and VIS Earth (Figure 1c) in the 12 May 2001 event. The frequency denotes the number of cases in which the difference was within the bins defined at the *x* axis. The thick lines compares boundaries for which the gaussian fit passed the *Carbary et al.* [2003] goodness of fit (GOF) tests. The thin lines are without GOF tests. Asterisks denote the frequency for boundaries in the [18–21] MLT sector (without GOF tests), which will be studied in more detail in section 4.2.

determined boundaries were rounded to the closest integer. The prominent boundaries were assigned an accuracy of ±1°, and the less clear boundaries were assigned an accuracy of ±2°. In the first images in the Southern Hemisphere, the oval was outside the field of view in a small region post-midnight. In these cases, the accuracy was set to ±3°. We used low altitude in-situ particle precipitation measurements from DMSP F12, F13, F14 and F15, as well as NOAA-15 (Table 1 shows these boundaries for the May 2001 event) to determine the boundary accurately when and where these satellites crossed the OCB.

[14] In Figure 1b and 1c, we compare our manually determined boundaries to boundaries determined by fitting the intensity profile to a gaussian, plus a quadratic polynomial which most often aligns with the background [*Carbary et al.*, 2003]. The thick lines show the frequency of differences between using the *Carbary et al.* [2003] method (including a goodness of fit (GOF) test), and our manual method. We see a fairly symmetrical distribution in the case of WIC, centered at 1–2°, indicating that we place our boundaries slightly equatorward compared to the *Carbary et al.* [2003] method. For VIS Earth, very few of the boundaries passed the *Carbary et al.* [2003] GOF tests. The thin lines show the difference when no test was applied on the fitted function. Many of these boundaries were still placed quite close to our manually determined boundaries, although this distribution is also centered at 1–2°. The seemingly common bias between manually determined boundaries and boundaries determined by gaussian fits, indicates that we have treated the two hemispheres equally, and that the resulting boundaries are comparable. The asterisks show the difference of the two methods in the [18–21] MLT region (without GOF tests). This region had particularly sharp poleward boundaries, and will be discussed in more detail in section 4.2. The automatic and manual methods seem to give similar results in this region, in the WIC images. The still present deviation seen in VIS Earth, is likely caused by a slant viewing angle in the equatorward edge of the auroral oval, distorting the fitted function. The slant viewing angle did however not affect the higher latitudes, and the boundary could be easily identified.

[15] We have also compared the manually detected OCBs to boundaries which were determined as the first point, from the pole, in which the intensity exceeds some threshold value. In 68% of the cases, our boundaries in the WIC images are within 2° of the boundaries determined by a threshold value of 800 counts. In VIS Earth, 83% of the boundaries were within 2° of the boundaries using a 25 counts threshold. The mentioned thresholds were the values giving the highest number of matches between the two methods. In the [18–21] MLT sector, these threshold boundaries matched the manually determined boundaries (within 2°) in 90% of the cases in WIC, and 93% of the cases in VIS Earth.

Table 1. Poleward Boundaries of Precipitation, as Seen by the DMSP and NOAA Satellites During the Time When WIC and VIS Observed the Entire Ovals in Both Hemispheres, During the 12 May 2001 Event

Satellite	UT	Mlat	MLT
DMSP-F15	21:32:30	−74.8°	20:50
NOAA-15	21:32:52	−70.6°	07:10
DMSP-F13	21:37:20	75.2°	18:00
NOAA-15	21:41:15	−79.5°	20:00
DMSP-F13	21:47:20	71.5°	07:50
DMSP-F14	21:56:49	78.9°	20:50
DMSP-F12	22:07:47	78.6°	20:00
DMSP-F15	22:16:45	77.0°	21:50

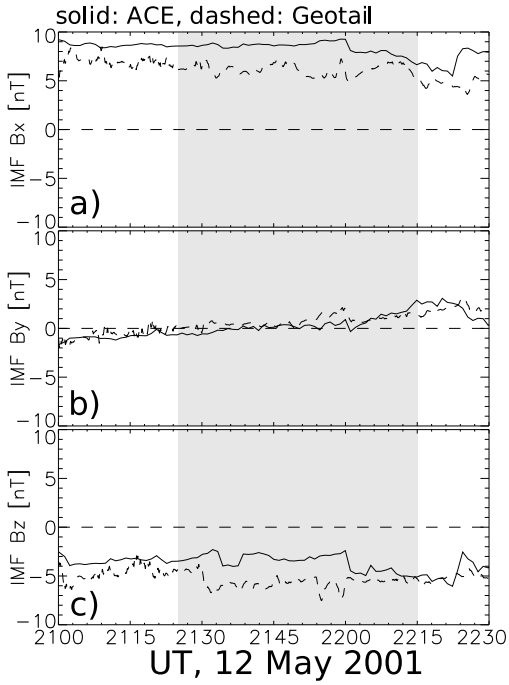

Figure 2. (a) IMF B_x, (b) B_y, (c) B_z, measured by ACE (solid) and Geotail (dashed) on 12 May 2001. The ACE measurements have been time shifted from its position in orbit around the L1 point to the Geotail position at $x_{GSE} = 12R_E$. The shaded region shows when IMAGE and Polar provided global coverage of the polar caps.

[16] Since some degree of subjectivity is impossible to avoid when the boundaries are determined manually, we include as auxiliary material print-outs of all images and boundaries from the 12 May 2001 event, for the sake of verifiability.[1]

[17] Figures 2a–2c show the IMF B_x, B_y, and B_z component during the May 2001 event. The dashed curves are measurements by Geotail, which was located at $(x, y, z)_{GSM} = (12, 8, 2)\ R_E$, and the solid curves are ACE measurements, time shifted to the Geotail position. The time shift, 52 minutes, was determined by a minimum variance analysis, and confirmed by matching a subsequent pressure increase (not shown) with its response in the geosynchronous magnetic field, measured by GOES-8. This is 15 minutes longer than $\Delta t = \Delta x/v_x$, which means that the phase fronts were oblique to the propagation [e.g., see *Haaland et al.*, 2007]. The solar wind speed and density (not shown) were constant at ≈620 km/s and ≈5 cm^{-3}, respectively, corresponding to a dynamic pressure slightly in excess of 3 nPa. The main point of Figure 2 is to emphasize the stable IMF orientation, with negative B_z, strongly positive B_x and almost zero B_y. The shaded region corresponds to the period with global coverage of the aurora in both hemispheres.

[1] Auxiliary materials are available in the HTML. doi:10.1029/2009JA015160.

3. Observations

[18] Figure 3 shows five pairs of simultaneous images in the Northern (upper row) and Southern (middle row) Hemispheres, starting at 21:27 UT, and spanning almost 40 minutes. The OCB is indicated by a red (black) curve in the Northern (Southern) Hemisphere. The ionospheric OCBs in the two hemispheres can be compared in the lower row. The UT at middle of exposure is shown above the images. All five pairs have some overlapping integration time. All images were taken during substorm expansion and recovery. The onset was seen in the Northern Hemisphere at 21 MLT at 21:24:55 UT (not shown).

[19] The first pair of images (Figure 3a) were taken a few minutes into the substorm expansion phase. At this time, the boundaries were quite circular and symmetric in the two hemispheres. As revealed in the images taken ten minutes later (Figure 3b), a large asymmetry between the hemispheres emerged as the boundaries propagated poleward. In the pre-midnight sector, the southern boundary was ≈5° closer to the pole than its northern counterpart, while neighboring regions (15 MLT and post-midnight) had an opposite asymmetry. Figure 3c shows that the asymmetry six minutes later, though still present, was more uniformly distributed in local time. At this time, the OCBs underwent rapid poleward propagation around 3 MLT. Eight minutes later (Figure 3d), the post-midnight region exhibited large asymmetries, the southern boundary being closer to the pole than the northern boundary duskward of 4 MLT, and further from the pole dawnward of 4 MLT. 12 minutes later (Figure 3e), the sense of the asymmetry was largely similar, demonstrating that the emerging asymmetries were relatively stable. The five pairs of images also show that the initial circular shape of the polar cap was better retained in the Northern Hemisphere when compared to the Southern Hemisphere.

[20] The images in Figure 3c reveal large differences in intensity distributions, as reported by *Laundal and Østgaard* [2009]. In section 4.5 we discuss how the non-conjugate spots may be interrelated with the spatial asymmetries in the magnetic field signified by the OCBs.

3.1. Interpretation in Terms of Open Magnetic Flux

[21] Previous studies have used auroral images to calculate the amount of open magnetospheric flux [e.g., *Milan et al.*, 2003; *Hubert et al.*, 2008]. Since $\nabla \cdot \mathbf{B} = 0$, the magnetic flux entering through the surface of the Earth is equal to the flux which is leaving the surface. Since the closed magnetic field lines by definition extend the same amount of magnetic flux in both hemispheres, the open field lines must also contain exactly the same amount of magnetic flux in the two hemispheres. Hence, conjugate global images can be used as a test of the hypothesis that the auroral oval circumvents all open magnetospheric flux: If the amount of flux in the two measured polar caps is different, the hypothesis or the method is wrong. The open flux is given as the surface integral $\int B_\perp dA$, where $B_\perp$ is the Earth's magnetic field perpendicular to the surface at ionospheric altitudes. We use the International Geomagnetic Reference

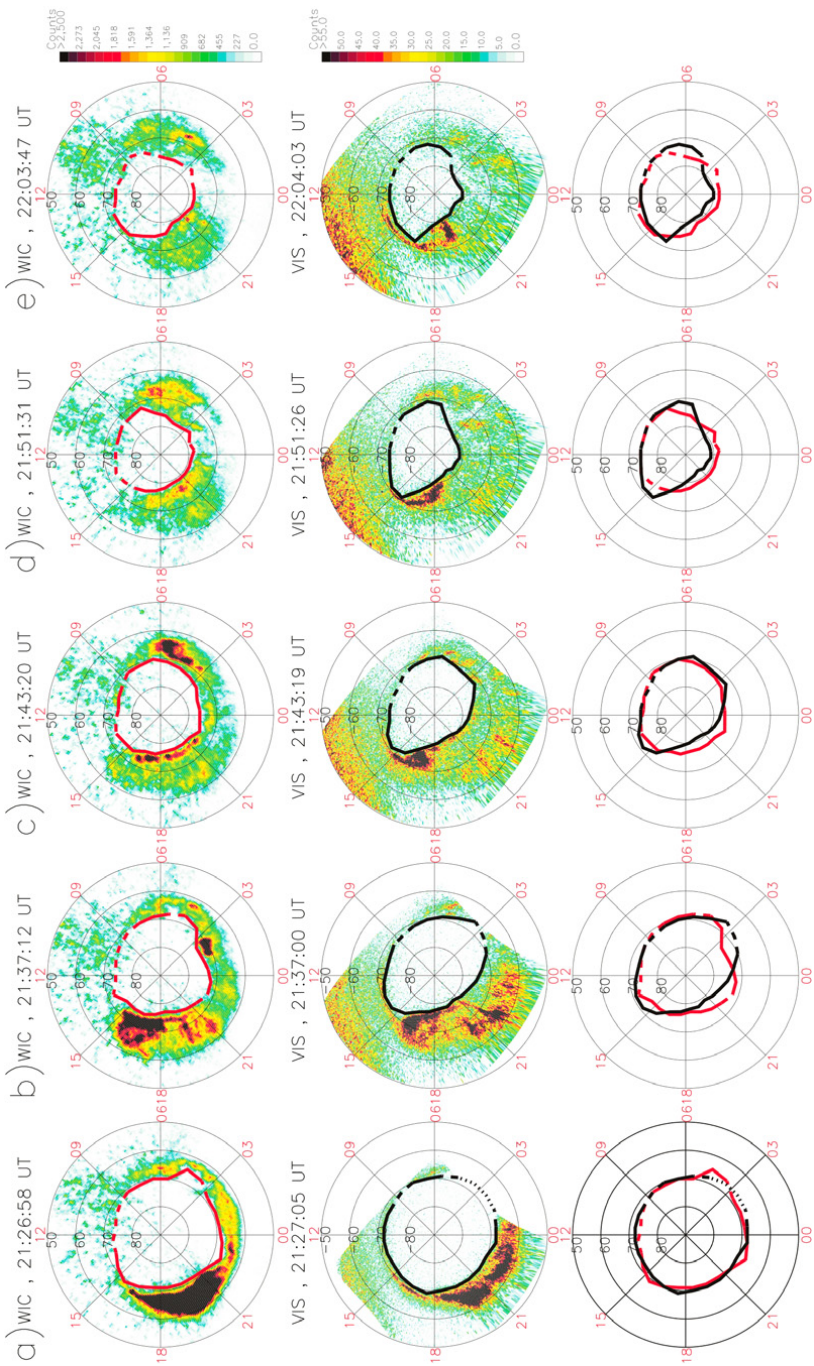

Figure 3. (a–e) Simultaneous images from the (top) Northern and (middle) Southern Hemisphere, with (bottom) the poleward boundary of the aurora in red (north) and black (south) shown in the images, and together for comparison. The UT of the middle of exposure is shown above the images. OCBs indicated by a solid line were clear and possible to determine independently. Dashed boundaries indicate less clear boundaries, and dotted lines are used where we have a lack of coverage (this was only the case for the post-midnight sector in the first images from the Southern Hemisphere).

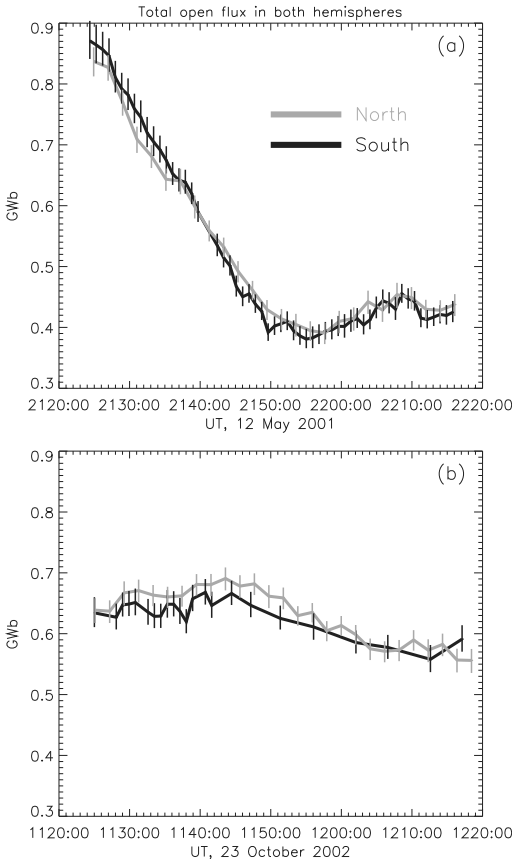

Figure 4. Total open flux in both hemispheres (a) 12 May 2001 and (b) 23 October 2002. The flux in the Northern (Southern) Hemisphere is shown in grey (black).

Field (IGRF) at 130 km altitude (the assumed emission height in the auroral images) for this purpose. The integration was performed in geographic coordinates.

[22] Figure 4 shows the total open flux in two hemispheres for the 12 May 2001 (Figure 4a) event, and from 23 October 2002 (Figure 4b). The latter event was studied in more detail by *Stubbs et al.* [2005]. The total open flux content can be written as a sum of the flux content in the 24 sectors, $\Phi = \sum_1^{24} \Phi_i$. With the assigned errors of 1, 2, or 3 degrees, each sector is associated with a corresponding error in the flux, $e^{\pm}_{\Phi,i}$, where superscripts + and − correspond to the error equatorward and poleward of the boundary, respectively. The total error of the flux was then calculated as $e^{\pm}_{\Phi} = \sqrt{\sum_1^{24}\left(e^{\pm}_{\Phi,i}\right)^2}$. Figure 4 shows that the measured amount of polar cap flux in the two hemispheres are similar for both events, within the applied error bars (i.e. they deviate by less than ≈0.05 GWb). This provides new evidence that the dim region encircled by the auroral oval, as seen by global FUV imaging, is indeed the ionospheric footprint of the open flux in the magnetosphere.

[23] We also notice that in the 12 May 2001 event, the initial amount of open flux in the magnetosphere was 0.85 GWb. *Milan et al.* [2008] showed that this number is high (the most probable value for open magnetic flux was ≈0.4 GWb in their study). According to *Milan et al.* [2009], the flux closure rate during substorms is high when the initial open flux content is high. This is also observed in the 12 May 2001 event, when ≈0.45 GWb closed in 25 minutes. This change in magnetic flux corresponds to a net mean closure rate of 300 kWb/s, or 300 kV.

[24] In Figure 5, we look in more detail at where, in terms of magnetic local time, the closing of flux took place in the 12 May 2001 event. Figure 5a–5d show the open flux content in six hours wide MLT sectors. Figure 5 clearly shows that in the first 15 minutes of the substorm, the closing of flux happened at the pre-midnight sector (d), followed by a steep drop in open flux content in the post-midnight sector (Figure 5a) during the following 10 minutes, in agreement with the observations of the OCB in Figure 3. This is consistent with tail reconnection happening in two steps, first at dusk and then at dawn, or that the X-line propagated from dusk to dawn. Figures 5a and 5d also show that the interhemispheric asymmetry appeared in conjunction with flux closure. More specifically, in the pre-midnight region (Figure 5d) an asymmetry appeared during the first 15 minutes, because the OCB moved poleward more rapidly in the Southern Hemisphere than in the Northern Hemisphere, resulting in more open flux in the Northern Hemisphere in this sector. Since the total open flux content is equal, an opposite asymmetry is expected elsewhere. This is observed post-midnight (Figure 5a) and (less clearly) post-noon (Figure 5c). In the following 10 minutes, when the closing of flux was most dominant post-midnight (Figure 5a), this region experienced a change in sign of the asymmetry. For the remaining period, the asymmetry was slowly reduced in the pre-midnight sector (Figure 5d). An opposite asymmetry, which balanced the total open magnetic flux content, was most clear pre-noon (Figure 5b). Because of the Poisson noise associated with the dayglow in the Northern Hemisphere, and the relatively low intensity of the dayside aurora in both hemispheres, an accurate determination of the boundary was difficult close to noon. As a consequence the asymmetries are generally within the error intervals in this region. However, the consistent behavior of the asymmetry seen between 21:30 and 21:40 in Figure 5c, and between 21:45 and 22:10 in Figure 5b, suggests that the asymmetries are real.

[25] In Figures 5e–5l we have divided the polar cap further into three hours wide MLT sectors. These plots show a more detailed picture of where the flux closed and how the interhemispheric asymmetries developed. Most prominently, the [0, 3] (Figure 5e) and [3, 6] (Figure 5f) MLT-sectors reveal that the asymmetry was much larger closer to midnight as the OCBs in this sector propagated poleward. After 21:50 UT, these sectors exhibited opposite asymmetries, which explains why the sum of these regions ([0, 6]), Figure 5a, was symmetric.

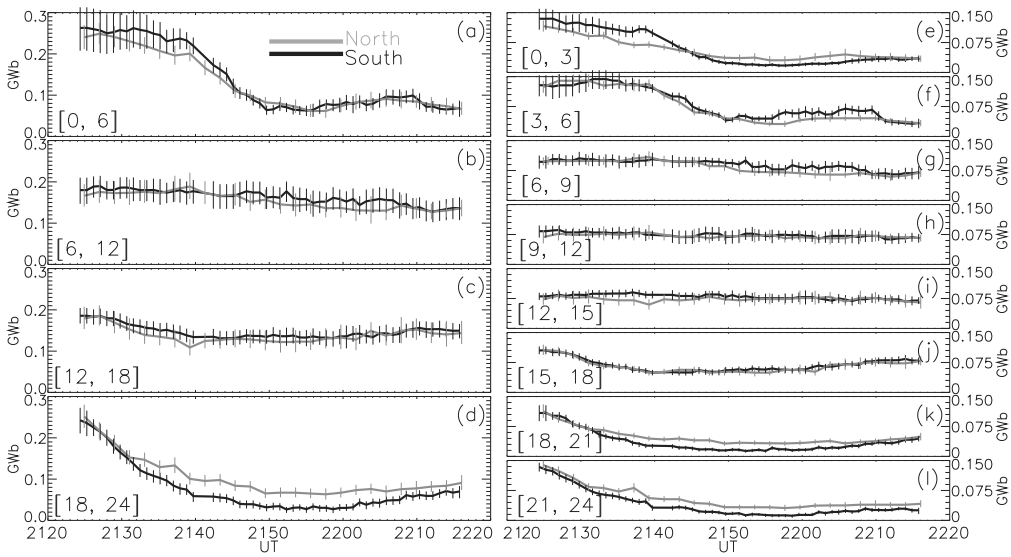

Figure 5. Open flux in different MLT sectors in both hemispheres (grey for the Northern Hemisphere, and black for the Southern Hemisphere). (a–d) Flux in 6 hours wide sectors, and (e–l) flux in 3 hours wide sectors. The error bars in Figure 5 are sums of the absolute errors, and hence relatively larger than the error bars in Figure 4.

[26] These observations show that auroral images from only one hemisphere is insufficient to determine local reconnection rate. In the [18, 24] MLT sector (Figure 5d), the reduction of magnetic flux differed by ≈50 MWb in the two hemispheres (20% of the initial flux content) during the first 20 minutes. Since the reconnection rate necessarily is equal in both hemispheres, this difference must be due to the emerging interhemispheric asymmetry.

4. Discussion

[27] The 50 minutes of global conjugate coverage of an auroral substorm presented in this paper reveals several interesting features: (1) The polar cap boundaries propagated poleward at different rates in the two hemispheres during the substorm expansion phase, leading to interhemispheric asymmetries in the polar cap boundaries. The interhemispheric asymmetry was as high as 5° in some regions. (2) The asymmetry differed from the classical view [e.g., *Cowley*, 1981a, 1981b] that polar cap asymmetries in essence is a global, uniform displacement. Instead, we observe that the asymmetry was largest in regions where the flux closure (tail reconnection) was strongest. Since the total open flux content must be the same in both hemispheres, such local asymmetries must be compensated for by an opposite asymmetry at other regions, which is what we observe.

[28] Comparing these findings to previous studies of interhemispheric asymmetries is problematic for two reasons. First, while many of the previous studies of interhemispheric asymmetries have focused only on the substorm onset location [*Østgaard et al.*, 2004, 2005b, 2007; *Liou et al.*, 2001], our findings show that interhemispheric asymmetries may change rapidly during the substorm expansion phase. This means that the formulas derived from onset observations [e.g., *Østgaard et al.*, 2004] may not be valid during the substorm expansion phase. A study of longitudinal asymmetries during the course of a substorm could resolve this issue. Second, studies which are restricted to local measurements of polar cap asymmetries [*Vorobyev et al.*, 2001] do not recognize the non-uniform nature in the asymmetry. For example, Figure 3b shows that if we were restricted to local measurements in one of the hemispheres, we would arrive at completely opposite conclusions, depending on which side of the magnetic midnight meridian we are.

[29] The only earlier study that has utilized conjugate images from IMAGE and Polar to study the entire auroral ovals, *Stubbs et al.* [2005], showed that the ovals (as represented by a best fit circle) were displaced in accordance with the expected B_y and B_x effects [e.g., *Cowley et al.*, 1991] and dipole tilt effect [e.g., *Oznovich et al.*, 1993]. Changes in asymmetry were seen to be directly related to changes in IMF orientation, consistent with newly opened field lines being subject to magnetic stresses [*Jørgensen et al.*, 1972]. The IMF control observed by *Stubbs et al.* [2005] is in contrast to the observations in the present paper, where large variations in asymmetry are seen, while the IMF remained fairly steady (Figure 2). The most obvious difference between the 12 May 2001 event, and the event studied by *Stubbs et al.* [2005], 23 October 2002 (Figure 4b), is the level of flux closure. The constant IMF and the rapid oval

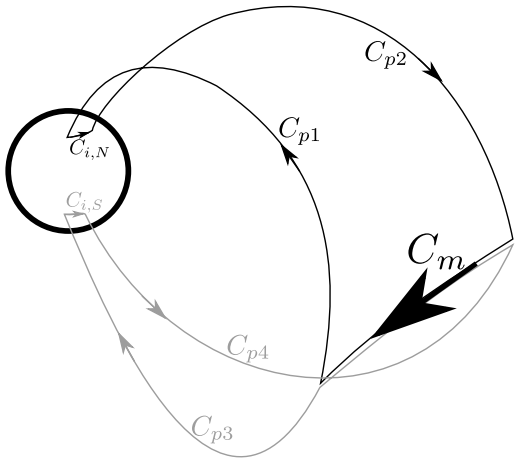

Figure 6. Paths of integration. C_m is along a segment of the X-line, and chosen so that it is similar for the two loops. The paths labeled C_p are along the magnetic field lines mapping from the X-line to the ionospheric footprints of the OCB, $C_{i,N}$ and $C_{i,S}$.

contraction suggests that the 12 May 2001 asymmetries were not directly driven by the IMF influence on newly open field lines, but rather by processes related to, or excited by tail reconnection.

[30] The progression of the OCBs from a symmetrical to an asymmetrical configuration implies that the boundaries moved at different velocities in the two hemispheres. In the following we show that the ionospheric OCB velocity depends on local reconnection rate, ionospheric convection velocity, and parallel electric fields. We also show how these quantities are related in a two-hemisphere system. Then we apply this relation on a segment of the OCBs in the 12 May 2001 event.

4.1. Open/Closed Boundary Motion

[31] The relation between polar cap motion and plasma convection can be found using a similar approach as proposed by *Vasyliunas* [1984] and applied in several reconnection studies [e.g., *Østgaard et al.*, 2005a]. We start with Faraday's law:

$$\oint (\mathbf{E} + \mathbf{u} \times \mathbf{B}) \cdot d\mathbf{l} = -\frac{\partial \Phi}{\partial t} \tag{1}$$

where Φ is the magnetic flux through a surface enclosed by the integration path on the left hand side. $\mathbf{u}$ is the velocity of the integration path with respect to the chosen coordinate system.

[32] Now we specify two integration paths, shown in Figure 6: $C_m + C_{p1} + C_{i,N} + C_{p2}$ and $C_m + C_{p3} + C_{i,S} + C_{p4}$, where $C_{i,N}$ and $C_{i,S}$ are along the ionospheric OCB in the Northern and Southern Hemispheres, respectively. C_m is along the segment of the X-line to which the two ionospheric paths map. The paths labeled C_p are chosen to be along magnetic field lines. For the integration paths C_p, $C_{i,N}$ and $C_{i,S}$ we assume the ideal MHD approximation to be true,

$$\mathbf{E} + \mathbf{v} \times \mathbf{B} \approx \mathbf{0}, \tag{2}$$

where $\mathbf{v}$ is the convection velocity of the plasma. A condition for this to hold is that the ion-neutral collision frequency is low. *Østgaard et al.* [2005a] showed that this requirement can be accommodated by placing the C_i integration paths at 300 km, which does not significantly change the latitudes inferred from auroral images (in which an emission height of 130 km were assumed). Equation (2) gives an expression for $\mathbf{E}$, which can be substituted in equation (1) everywhere, except along C_m. The integrand then, $([\mathbf{v} - \mathbf{u}] \times \mathbf{B}) \cdot d\mathbf{l}$, vanishes along C_p, since $\mathbf{B}$ is parallel to $d\mathbf{l}$. If $E_\parallel \neq 0$, equation (2) does not hold along C_p, but the integrals along the C_p's would cancel if the potential drop along these paths are the same. In section 4.3 we discuss the effect of non-canceling parallel electric fields. The integration path is chosen so that it is tangent to the magnetic field, and $d\Phi = \mathbf{B} \cdot \mathbf{n} dS$ is identically zero everywhere. Therefore the magnetic flux threading the surface is zero, and thus constant, and the right hand side of equation (1) vanishes. Since $\mathbf{B}$ is either parallel to the X-line or zero, $\mathbf{u} \times \mathbf{B} = \mathbf{0}$ along C_m. Hence, equation (1) reduces to

$$\int_{C_m} \mathbf{E} \cdot d\mathbf{l} = \int_{C_i} ([\mathbf{v} - \mathbf{u}] \times \mathbf{B}) \cdot d\mathbf{l}. \tag{3}$$

For the C_i integration path, $\mathbf{u}$ corresponds to the velocity of the ionospheric open/closed boundary. $\mathbf{v}$ is the ionospheric convection velocity.

[33] This equation demonstrates that, if there is no reconnection in the magnetosphere ($\mathbf{E} = \mathbf{0}$ on the left hand side), $\mathbf{u} = \mathbf{v}$, and the open/closed boundary moves exactly with the plasma convection (adiaroic convection). The equation also shows the equivalence between magnetic reconnection rate, quantified by $\mathbf{E}$, and plasma flow across the OCB, $\mathbf{v} - \mathbf{u}$ [*Vasyliunas*, 1984]. This identity has previously been used to assess tail reconnection rate from combined measurements of OCB location and plasma flow [e.g., *de la Beujardiere et al.*, 1991; *Blanchard et al.*, 1996; *Østgaard et al.*, 2005a; *Hubert et al.*, 2008].

[34] The left hand side of equation (3) is common for both paths of integration depicted in Figure 6, since conjugate segments of the OCB map to the same X-line. Setting the right hand sides in the two equations (for the two integration paths) equal to each other, we get the relation between ionospheric convection, open/closed boundary motion, and magnetic field in the two hemispheres:

$$\int_{C_{i,N}} ([\mathbf{v} - \mathbf{u}] \times \mathbf{B}) \cdot d\mathbf{l} = \int_{C_{i,S}} ([\mathbf{v} - \mathbf{u}] \times \mathbf{B}) \cdot d\mathbf{l}. \tag{4}$$

[35] From this equation it is clear that if the ionospheric convection $\mathbf{v}$ is different in the two hemispheres, $\mathbf{u}$ may also be different, and the OCBs may become asymmetrical. However, this statement is not yet exact, since interhemispheric differences in $\mathbf{v}$ may also be balanced by differences in $\mathbf{B}$, and by differences in the integration paths. We thus

need to make further considerations in order to use this equation quantitatively.

[36] First, we make one approximation regarding the integration paths: Let C_i coincide with circles of magnetic latitude (the OCB is circular along C_i seen in magnetic coordinates). We then introduce average values of the quantities in the integrand, in order to solve the integral:

$$\int_{C_i} ([\mathbf{v}-\mathbf{u}]\times\mathbf{B})\cdot d\mathbf{l} = LB_{\perp}(v-u) \tag{5}$$

$$\Rightarrow L_N B_{\perp,N}(v_N-u_N) = L_S B_{\perp,S}(v_S-u_S) \tag{6}$$

where L is the length of C_i, $B_\perp$ is the absolute magnetic field perpendicular to $d\mathbf{l}$, and v and u are velocities in the equatorward direction along magnetic meridians (the velocities are assumed to be horizontal).

[37] In general, $B_{\perp,N} \neq B_{\perp,S}$ and $L_N \neq L_S$, even when the OCB segments are on the same magnetic latitude. This is because the Apex coordinate system (and also the similarly defined AACGM system) is irregular: In the region above 60° magnetic latitude, the geographic distance corresponding to one degree of magnetic latitude ranges from ≈93 km (≈97 km) to ≈131 km (≈165 km) in the Northern (Southern) Hemisphere. The length of one degree of magnetic longitude will also vary along a circle of magnetic latitude.

[38] Conjugate images give us an estimate for the OCB locations, which we can differentiate to get the OCB velocity. The resulting unit is magnetic latitude per second, which, according to the previous paragraph is not proportional to m/s. In order to take this effect into account, we transform equation (6) to magnetic coordinates. To do this, we recognize that the OCB velocity, u', measured in magnetic coordinates relates to the OCB velocity in equation (6), u, by $u' = u/d$, where d is the dimensionless ratio between a unit length along a meridian in the magnetic system (not constant), and a (constant) unit length in a regular system (e.g., the length of one degree magnetic latitude, divided by the length of one degree latitude in a regular system, $2\pi R_E/360$). Similarly, $v' = v/d$. As discussed above, d is a function of space (on the surface of the Earth). From now on, primed quantities refer to quantities measured in magnetic coordinates. Multiplying equation (6) by $\frac{d_N d_S}{d_N d_S}$, we get,

$$d_N L_N B_{\perp,N}(v'_N-u'_N) = d_S L_S B_{\perp,S}(v'_S-u'_S) \tag{7}$$

$$\Rightarrow \Phi_N(v'_N-u'_N) = \Phi_S(v'_S-u'_S) \tag{8}$$

where we have interpreted $dLB_\perp$ as the magnetic flux Φ in a thin strip along the OCB of length L and width d (since d is dimensionless, we will have to multiply the equation by a unit length to justify this). An advantage of the Apex (and AACGM) coordinate system is that the magnetic flux in areas spanned by the same magnetic coordinates in the two hemispheres, is equal. This means that, if the OCBs start out being symmetrical, so that $\Phi_N = \Phi_S$, equation (8) implies that they can become asymmetrical ($u'_N \neq u'_S$) only if $v'_N \neq v'_S$. Emerging OCB asymmetries thus presupposes differences in the ionospheric equatorward convection in the two hemispheres.

[40] If, on the other hand, the OCBs are on different latitudes, $\Phi_N \neq \Phi_S$ (assuming they span the same longitudinal angle). In the Apex/AACGM systems, the amount of magnetic flux in equally wide concentric circles diminish towards the pole (in the longitudinal direction, the flux content is constant in these circles). A consequence of this can be seen if we put the convection equal to 0 in both hemispheres, so that the OCB moves only in response to magnetic reconnection. Then, $u'_S = \frac{\Phi_N}{\Phi_S}u'_N$. If, say the southern OCB is poleward of the northern OCB, $\Phi_N > \Phi_S$, and the southern OCB will move faster than the northern OCB. Hence, if the ionospheric footprints of an X-line in the tail (flux closure) are on different latitudes, the asymmetry will be reinforced. We emphasize that this is more of a geometric effect, introduced by the definition of the Apex coordinates, rather than an increase in the field line distortion. Nevertheless, this property must be taken into account here, and it is also useful to be aware of, since it implies that latitudinal asymmetries may be self-reinforcing. If the asymmetry is measured in magnetic flux, as in Figure 5, the self-reinforcement effect is compensated for.

4.2. OCB Motion: The 12 May 2001 Event

[41] We now solve equation (8) for the [18, 21] MLT sector in the 12 May 2001 event. The conjugate images have given us the average OCB location, from which we can find u'_S and u'_N, and calculate Φ_N and Φ_S. All quantities are considered as constant along the OCB segment. We also need to assume that the two segments of the OCB are indeed conjugate, and not displaced in longitude. To get the difference in ionospheric convection from equation (8), we will have to make assumptions for the convection velocity in one of the hemispheres. These assumptions necessarily introduce significant errors. However, the purpose of this exercise is to give a rough assessment of what the ionospheric convection must be, in order to account for the observed asymmetries. The choice of the [18, 21] sector is due to its prominent OCB, large asymmetry, and the fact that two DMSP spacecraft, carrying instruments which could measure the plasma convection, crossed the OCB in the two hemispheres. We will use these measurements, and physical considerations, to substantiate our estimate of the convection.

[42] The quantities in equation (8) for the [18, 21] MLT sector are shown schematically in Figure 7. Figure 8a shows the average location of the OCB in this sector (thin, solid), with error (dashed). We have interpolated the values to a common time resolution, and then calculated four minutes averages (thick, solid). The Northern Hemisphere boundaries are shown in grey, and the Southern Hemisphere in black. The change in latitude over time gives u' for both hemispheres, shown in Figure 8b. u' is shown in units of m′/s = (m/d)/s, where d is the scaling factor described in section 4.1. At the OCBs considered in Figure 8, d is close to 1 ($d \in [0.93, 1.12]$), so that m′/s is always close to m/s. However, we keep the primes for consistency with the preceding section, and to emphasize the principal difference between the magnetic coordinate system and a regular coordinate system. Figure 8b shows that the poleward velocity of the southern OCB is higher than the poleward velocity of the northern OCB, which leads to the observed increasing asymmetry. Figure 8c shows the evolution of Φ_N/Φ_S (in our calculation, we used the magnetic flux within a strip with a width of 1° magnetic latitude, centered at the OCB latitude). The ratio is 1 where the OCBs are collocated,

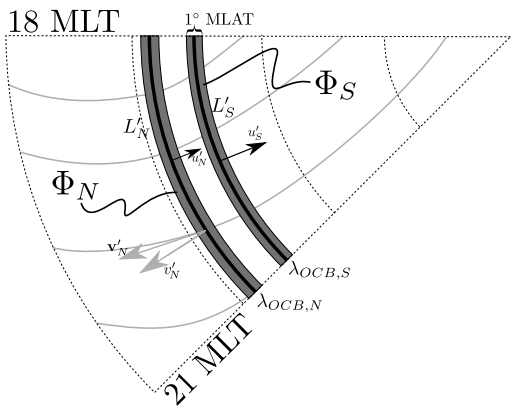

Figure 7. Schematic illustration of the quantities in equation (8). The OCB motion, u' is derived from measurements of the OCB location (λ_{OCB}). This motion depends on reconnection rate, and ionospheric convection. An illustration of the convection pattern is shown as grey contours (for clarity, only one hemisphere is shown). v' is the projection of the ionospheric convection $\mathbf{v}'$ onto a magnetic meridian. The grey strips along the OCBs mark the regions containing the flux Φ_N and Φ_S in equation (8) (for numerical reasons, we used a width of 1° magnetic latitude for the strips). Figure 7 is shown in magnetic coordinates, and for consistency with the text, we use primes to denote quantities which can take different values when transformed to a geographic coordinate system (except for λ_{OCB}).

and otherwise in agreement with decreasing magnetic flux towards the pole.

[43] The unknown quantities in equation (8) are v'_S and v'_N. First we consider the case that $v'_S = v'_N$. The resulting convection velocity is shown in Figure 8d. During the first ten minutes, the convection is unrealistically strong. This is a strong indication that the equatorward ionospheric convection must have been different in the two hemispheres during this period. After 21:35 UT, the convection is reduced, but still relatively strong (fluctuating between ≈−500 m′/s and ≈2500 m′/s). This behavior is also unrealistic, but considering the inherent uncertainties in our method, we can not rule out the possibility of symmetrical (or almost symmetrical) convection during the last 10 minutes of the period.

[44] In order to obtain some reasonable value, we will set the convection in one hemisphere to a fixed positive (equatorward) value, and then use equation (8) to calculate the other. In Figure 8e, the grey lines show v'_N = 600 m′/s (dashed) and v'_N = 900 m′/s (solid). The corresponding convection in the Southern Hemisphere is shown as black curves. In both cases, the asymmetry between hemispheres is strong ($\Delta v' \sim$ 500 m′/s) in the first ten minutes, and smaller towards the end. This shows that a difference in v of ≈500 m′/s, lasting for ≈10 minutes can account for the observed asymmetries. The decrease in equatorward convection seen in the Southern Hemisphere does however seem unreasonable, considering the increase observed in previous studies of ionospheric convection during substorm expansion [e.g., *Provan et al.*, 2004].

[45] We now use convection measurements from the two OCB crossings by DMSP F15 and F13, as well as the results from Figures 8d and 8e to suggest a more realistic scenario. The convection measurements are shown in Figure 9. Figures 9c and 9d show the value of the convection vector composed from the RPA (parallel to the satellite track) and IDM (perpendicular to the track) measurements projected onto a magnetic meridian in the Northern and Southern Hemispheres, respectively (positive in the equatorward direction). The vertical dotted bars show the time when the spacecraft crossed the OCB, as determined by particle precipitation measurements (Table 1). The values are averages within 40 seconds bins (the nominal resolution is 4 seconds), and the vertical bars denote the standard error. Only measurements labeled "good" were used for this purpose. From Figure 9, we get that $v_S \approx$ 300 m/s at 21:32:30 UT, and $v_N \approx$ 600 m/s at 21:37:20 UT (diamonds in Figure 8f). Figures 9a and 9b show the velocity vectors along the satellite tracks, plotted on top of the auroral images closest to the OCB crossing. In Figures 9a and 9b, the blue vectors denote measurements of "good" quality, while the red vectors include measurements labeled "caution."

[46] In Figure 8f, we assume the convection in the Northern Hemisphere to increase from 0 m′/s to 900 m′/s in the first few minutes of the period, and decrease to 600 m′/s at 21:35 UT. These velocities were chosen for two reasons: First, it does not imply a reduction of the convection in the Southern Hemisphere during the first ten minutes (as opposed to the v_N = const. case). Second, the velocities at the times of the OCB crossings by the DMSP spacecraft were chosen so that they are in accordance with the measurements ($d \approx 1$ so that m′/s ≈ m/s). This scenario confirms that an interhemispheric difference in equatorward convection of ≈500 m/s (using $d \approx 1$) during the first 10 minutes of the period can account for the observed asymmetry. During the remaining period, much of the still growing asymmetry is handled by the self-reinforcement effect discussed in the previous section. However, some rather fluctuating differences in convection seem to remain.

4.3. Effect of $E_\parallel$

[47] So far we have assumed $E_\parallel = 0$ along the C_p integration paths, so that equation (2) is valid. If we allow for parallel electric fields to be present, the integrals along C_p become $\int_{C_p} E_\parallel dl = \Delta V$, since the remaining terms in the integrand in equation (1) are perpendicular to $d\mathbf{l}$. If the potential drop along the two C_p's are equal, the effect of parallel electric fields are canceled by the opposite directions of the integration paths. If, on the other hand, there is a spatial gradient perpendicular to the magnetic field in the electric potentials, so that the two field aligned integrals do not cancel, we are left with a net potential drop in addition to the terms in equation (3). Assuming this net potential drop is only present in one hemisphere, we can follow the same procedure as derived above, and arrive at equation (8), only with the potential drop ΔV at one side of the equality,

$$d_N L_N B_{\perp,N}(v'_N - u'_N) = d_S L_S B_{\perp,S}(v'_S - u'_S) + \Delta V \qquad (9)$$

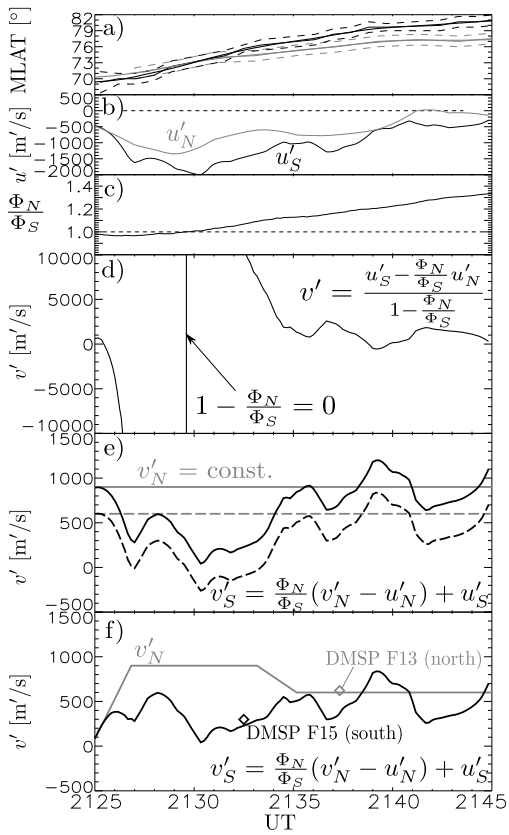

Figure 8. Equation (8) solved for the [18, 21] MLT sector on 12 May 2001. (a) Magnetic latitude of the OCB in the Northern (grey) and Southern (black) Hemispheres. The thick curves were averaged over four minutes. The dashed curves show the uncertainty. (b) OCB equatorward motion. The unit is m′/s = (m/*d*)/s. (c) Ratio of the magnetic flux in thin strips along the OCBs, Φ_N/Φ_S. (d) Equatorward convection velocity, assuming $v'_N = v'_S$. (e) Equatorward convection velocities in the south, assuming v'_N = 600 m′/s (dashed) and v'_N = 900 m′/s (solid). (f) Equatorward convection velocity in the south, assuming the convection in the Northern Hemisphere follows the grey curve. The diamonds mark convection measurements by two DMSP spacecraft.

For the dimensions to be consistent, we write the Φ's as $dLB_\perp$. This equation implies that, to accommodate the potential drop, plasma must be allowed to cross magnetic field lines (v' - $u' \neq 0$, at least in one of the hemispheres), in such a way that differences in u' may be introduced between hemispheres. If, for simplicity, we assume $d_N L_N B_{\perp,N} = d_S L_S B_{\perp,S} = LB_\perp$ and $v_N = v_S$ (we skip the primes now, since d is assumed to be 1), and let ΔV be positive (this could correspond to an electric field anti-parallel to the C_{p3} integration path (parallel to the magnetic field) in Figure 6), equation (9) gives the difference between u_N and u_S introduced by the potential drop:

$$u_N - u_S = \frac{\Delta V}{LB_\perp}. \tag{10}$$

For a magnetic field of 50,000 nT and $L \approx 2000$ km (which corresponds approximately to a longitude segment of 45° at 75° latitude), we get $LB_\perp \approx 100$ Tm. For a parallel potential drop of 5 kV, this corresponds to a difference between u_N and u_S of 50 m/s. If this was allowed to go on for 20 minutes, it would result in an interhemispheric asymmetry of ≈0.5°. A difference in u of 50 m/s is thus much less than the typical differences observed in Figure 8b. However, it should be noted that this is an average value for the entire 45° wide sector. If we reduced L, thus sharpening the gradient in ΔV, the difference in u would grow, and could become a significant factor in producing local interhemispheric field line asymmetries.

4.4. Asymmetric Convection

[48] The scenario suggested by Figure 8f is that the observed asymmetry in the 18–21 MLT sector in the 12 May 2001 event can be accounted for by a brief (~10 minutes) period of asymmetrical meridional convection ($\Delta v \approx 500$ m/s) in the two hemispheres. The next question is why the convection becomes asymmetric. In very general terms, the answer to this question is that either the high-altitude (magnetospheric) region, which is the ultimate source of the ionospheric convection, enforces the asymmetry, or that the ionosphere responds differently to symmetrical forcing, or a combination of these effects. In the 12 May 2001 event, two parameters which are believed to contribute in separate regions stand out: 1) The IMF B_x component was strong (B_y was not), which, according to *Cowley* [1981b] can lead to asymmetrical lobes, forcing the equatorial plane in the negative z direction. Owing to the same forces, the northern half of the field lines might be expected to be pushed inward more efficiently, leading to the convection asymmetry. However, this can not be the sole cause, since the OCBs became asymmetric while the IMF was unchanging. 2) The Northern Hemisphere was highly sunlit, and the Southern Hemisphere was in darkness. The situation depicted in Figure 8f resembles a northern, sunlit hemisphere which responds promptly to a burst of earthward magnetospheric convection, while the southern winter ionosphere lags behind. The difference in ionospheric response could be due to an excess of parallel electric fields in the southern winter hemisphere compared to the summer hemisphere [e.g., *Newell et al.*, 1996], which could decouple the southern ionosphere from the magnetosphere. Another possibility is that the pre-existing convection in the northern summer hemisphere, which according to statistical studies [*Ruohoniemi and Greenwald*, 2005] of ionospheric convection should be stronger than in the winter hemisphere, more easily accommodates the change in magnetospheric convection. The increased meridional convection imposed by the magnetosphere, which these explanations presuppose, has been shown to be characteristic of the substorm expansion phase [*Provan et al.*, 2004; *Bristow and Jensen*, 2007]. The Northern Hemisphere flow in Figure 8f is stronger than typical observations reported by *Provan et al.* [2004] and

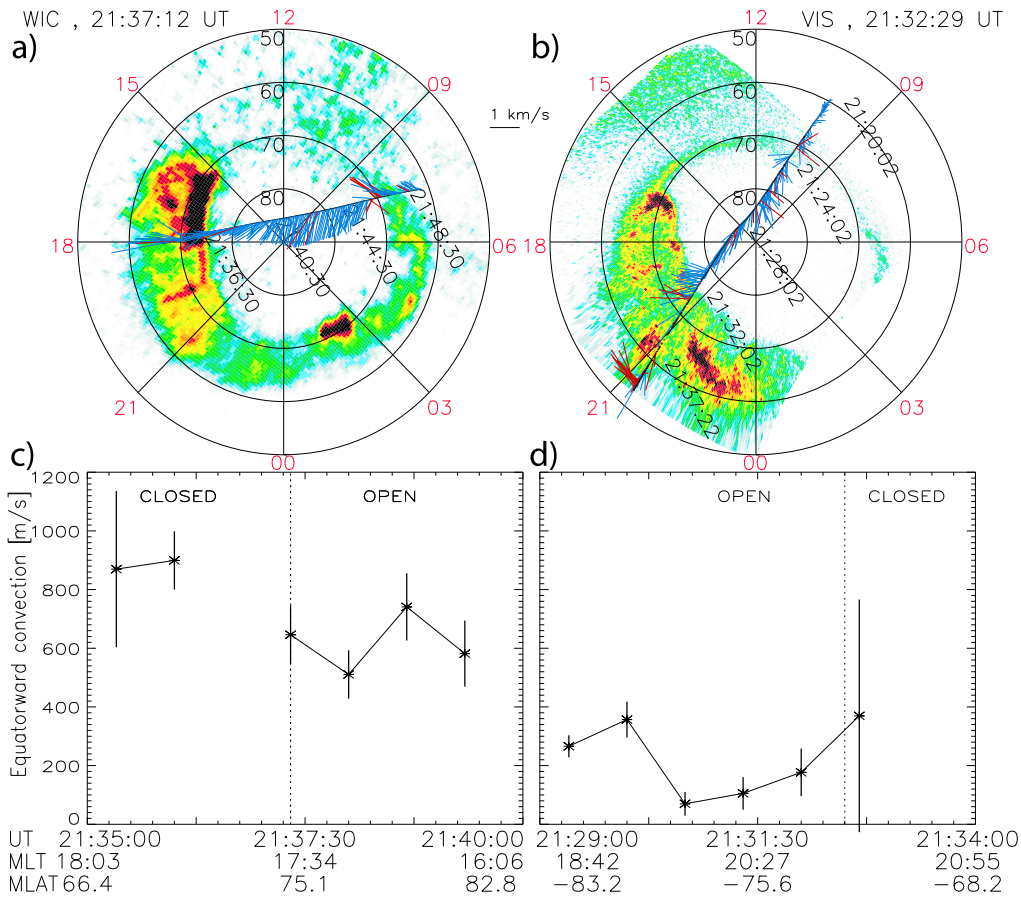

Figure 9. Ionospheric convection measurements from DMSP F13 and F15. (a) WIC image from the Northern Hemisphere, taken approximately at the time when DMSP F13 crossed the open/closed boundary at the dusk side. Horizontal convection measurements along the satellite track is also shown. Blue color indicates data of good quality, while the red vectors include data labeled "caution". (b) Same format as Figure 9a, but with satellite track of DMSP F15, which crossed the southern OCB at dusk approximately when the image was taken. (c) Average convection velocity in the Northern Hemisphere projected onto a magnetic meridian (positive in the equatorward direction). Each data point is an average of the ("good") measurements obtained at the UT on the x-axis ± 20 seconds. The error bars show $s/\sqrt{n}$, where s is the standard deviation, and n (≥2) is the number of measurements. The vertical dotted bar marks the time of the OCB crossing. (d) Same format as in Figure 9c, but for the Southern Hemisphere (DMSP F15).

Bristow and Jensen [2007], but still at a reasonable level, considering the above average strength of the substorm.

[49] The increased meridional flow is also in accordance with the theory by *Cowley and Lockwood* [1992], who proposed that the destruction of open flux implied by tail reconnection leaves the magnetosphere-ionosphere system in an excited state, which is then brought back towards an equilibrium by convection, thus making reconnection a key prerequisite for convection. This concept is illustrated in Figure 10, which is a copy of *Cowley and Lockwood* [1992, Figure 7]. In Figure 10a, there is no generation or destruction of open magnetic flux, and consequently, there is no flow across the OCB. In Figure 10b, impulsive reconnection in the tail has closed an amount of flux, dF, causing the ionospheric footprint of the X-line to move to higher latitudes. The convection, which has not yet commenced, will now start to transport the OCB to the new equilibrium, shown as a dotted-dashed circle. The excited convection is shown as arrowed loops in Figure 10c. In this panel, the reconnection has ceased, and the OCB is transported

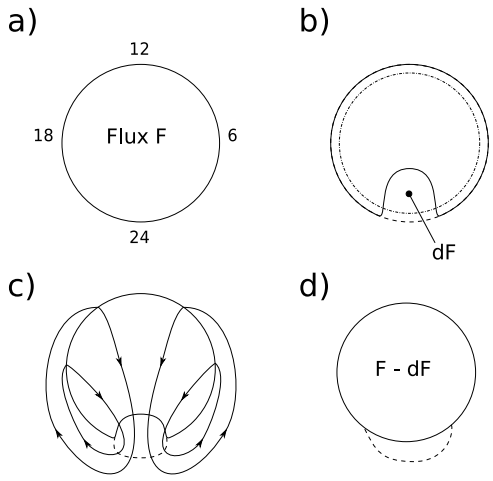

Figure 10. Cartoon showing how ionospheric convection is excited after magnetic flux closes. The solid curves indicate the open/closed field line boundary. (a) Static situation, in which no flux is opened on the dayside or closed on the nightside, and consequently there is no convection. The total open flux content is *F*. (b) Impulsive tail reconnection has closed flux (*dF*), causing a perturbation to the boundary. The dashed-dotted line indicates the new equilibrium OCB. (c) The tension associated with the perturbed boundary in the magnetosphere excites convection (arrowed solid loops), transporting the OCB towards a new equilibrium. The dashed curve indicates the boundary of the closed flux. (d) A new equilibrium has been achieved. The dashed curve indicates the location of the redistributed, newly closed flux. Figure 10 is a copy of *Cowley and Lockwood* [1992, Figure 7]. With kind permission of Springer Science + Business Media.

towards the new equilibrium with the flow (**u** = **v** in equation (3)). The new equilibrium is reached in Figure 10d, and the convection has stopped. The closed flux, *dF* has been redistributed to the area indicated by the dashed curve. In reality, this process happens more continuously, and the presence of reconnection on the dayside and on the nightside is what leads to the familiar two-cell convection pattern.

[50] According to this picture, the magnetospheric convection should be strongest where the reconnection is strongest. Therefore, due to differences in the ionospheric response, interhemispheric asymmetries in the OCB might also be expected to be strongest in these regions. This is in excellent agreement with the observations presented in Figure 5, which shows that the asymmetry is strongest in the regions where more flux closes. The conspicuously more circular OCBs in the northern than in the Southern Hemisphere (Figure 3) might also be explained in terms of the Figure 10 cartoon; if the Northern Hemisphere responded more promptly to the magnetospheric convection excited after flux closure in the tail, the ionospheric OCB would reach equilibrium (circle) earlier than in the Southern Hemisphere. In this process, the elevated convection in the Northern Hemisphere, will also transport the OCB at the regions flanking the X-line to relatively lower latitudes, which may explain the opposite asymmetries at dawn and dusk.

4.5. OCB Asymmetries and Interhemispheric Currents

[51] The 12 May 2001 event also exhibited non-conjugate aurora which has been interpreted as ionospheric signatures of interhemispheric currents [*Laundal and Østgaard*, 2009]. One of the non-conjugate spots occurred at the dawn side in the Northern Hemisphere, between 21:40 and 21:50 UT. This coincides remarkably well with significant flux closure in this region (Figure 5a), and a concurrent change in asymmetry (most evident in Figure 5e). This strongly suggests that the current and the field line perturbations signified by the OCB asymmetries are interrelated. The simplest realization of the field line perturbation, is to consider the field lines to be deformed only in the radial direction. In that case, the OCB asymmetry on the dawnside is consistent with an additional perturbation magnetic field in the outward direction, while the nightside asymmetry is consistent with an inward perturbation field. By Ampere's law, the shear in the perturbation field between these regions implies a current anti-parallel to the field lines (electrons down in the Northern Hemisphere), approximately collocated with the non-conjugate dawn spot in the north. Since in large-scale space plasmas, the curl in magnetic field in general produces the current, and not vice versa [*Parker*, 1996; *Vasyliunas*, 2005], the cause for the non-conjugate spot (which signifies a current) may therefore be found if we can explain the OCB asymmetry (which signifies $\nabla \times \mathbf{B}$).

[52] To this end, we need to know the parameters which govern the convection during the substorm expansion phase, and hence the emerging asymmetries in the magnetic field. We have pointed out two possible candidates in the 12 May 2001 event: The IMF B_x, and the dipole tilt angle (through interhemispheric differences in ionospheric conductivity). To properly address this question, more statistics is needed. Because of the lack of global conjugate images, the most practicable way of doing this is by MHD modeling, or by a superposed epoch analysis of substorm observations in one hemisphere. This is reserved for a future work.

5. Conclusions

[53] We have used two serendipitous constellations of the IMAGE and Polar spacecraft, both equipped with UV imagers, to study the conjugate auroral ovals. We have focused on the size and shape of the dim region encircled by the bright aurora. The magnetic flux content in these regions were found to be equal. This indicates that the polar caps, as observed in UV images, are cross sections of the open magnetic flux, as is often assumed.

[54] In one of the events, 12 May 2001, a significant amount of flux closed during the expansion phase of a substorm. Concurrently, the open/closed boundary in the two hemispheres became highly asymmetrical. The emerging asymmetries were strongest in the regions where magnetic flux closed most rapidly. In neighboring regions, an opposite asymmetry was observed, preserving equal amounts of open flux.

[55] These observations strongly suggest that the interhemispheric asymmetry at the footprints of the magnetic field lines increases, and hence the magnetic field is deformed during the course of a substorm. This has not been recognized in previous studies of interhemispheric symmetry. The local nature of the asymmetries seen in this study implies that local measurements of the asymmetry may give an incomplete view of magnetospheric geometry. A complete view of interhemispheric asymmetries, and hence its causes, can only be given if temporal and spatial variations are considered.

[56] We have shown that open/closed boundary asymmetries can only arise if the ionospheric convection velocities are different in the two hemispheres, or in the presence of spatial gradients in field aligned electric potential drops along the OCB. A quantitative analysis of the [18, 21] MLT sector revealed that most of the emerging asymmetry in this sector could be accounted for if the ionospheric convection in the meridional direction differed by ≈500 m/s in the two hemispheres for the first ~10 minutes of the expansion phase. We suggest that the cause for the different convection velocities are differences in the ionospheric response to an increase in magnetospheric convection during the substorm expansion phase. The difference in ionospheric response can be due to the large seasonal differences. The strong B_x component in the IMF could also contribute to an OCB asymmetry [*Cowley*, 1981a], although this effect seems less likely, since the IMF remained almost constant, while the asymmetries changed rapidly.

[57] The clear dependence of the OCB asymmetry on reconnection rate (Figure 5) suggests that the observations presented in this paper represent an intrinsic phenomenon during substorm expansions, when flux closes rapidly in the tail [e.g., *Milan et al.*, 2009]. We have identified the IMF and ionospheric conductivity differences in the two hemispheres as two potential sources for the asymmetry. In other events, when $B_y \neq 0$, we might expect polar cap asymmetries to appear under the influence of the different flow strengths in the two convection cells [*Provan et al.*, 2004]. However, to firmly determine the parameters responsible for the asymmetries, more statistics is needed.

[58] **Acknowledgments.** The authors thank S.B. Mende and the IMAGE FUV team for the use of IMAGE FUV data. We thank J. Sigwarth for the use of Polar VIS Earth data. We thank C. Smith for the ACE magnetic field data and D. McComas for the ACE solar wind data. We gratefully acknowledge the Center for Space Sciences at the University of Texas at Dallas and the U.S. Air Force for providing the DMSP thermal plasma data. The DMSP boundaries were determined from plots at The Johns Hopkins University Applied Physics Laboratory web page. Marit Sandanger and Finn Søraas assisted in the processing of NOAA data. Geotail magnetic field data were provided by T. Nagai through DARTS at Institute of Space and Astronautical Science, JAXA in Japan. This study was financed by the IPY-ICESTAR project, The Research Council of Norway, contract 176045/S30.

[59] Masaki Fujimoto thanks the reviewers for their assistance in evaluating this paper.

References

Blanchard, G. T., L. R. Lyons, O. de la Beaujardiére, R. A. Doe, and M. Mendillo (1996), Measurement of the magnetotail reconnection rate, *J. Geophys. Res.*, *101*, 15,265–15,276.

Boakes, P. D., S. E. Milan, G. A. Abel, M. P. Freeman, G. Chisham, B. Hubert, and T. Sotirelis (2008), On the use of IMAGE FUV for estimating the latitude of the open/closed magnetic field line boundary in the ionosphere, *Ann. Geophys.*, *26*, 2759–2769.

Boakes, P. D., S. E. Milan, G. A. Abel, M. P. Freeman, G. Chisham, and B. Hubert (2009), A statistical study of the open magnetic flux content of the magnetosphere at the time of substorm onset, *Geophys. Res. Lett.*, *36*, L04105, doi:10.1029/2008GL037059.

Bristow, W. A., and P. Jensen (2007), A superposed epoch study of SuperDARN convection observations during substorms, *J. Geophys. Res.*, *112*, A06232, doi:10.1029/2006JA012049.

Brittnacher, M., M. Fillingim, G. Parks, G. Germany, and J. Spann (1999), Polar cap area and boundary motion during substorms, *J. Geophys. Res.*, *104*, 12,251–12,262, doi:10.1029/1998JA900097.

Burch, J. L. (2000), IMAGE Mission Overview, *Space Sci. Rev.*, *91*, 1–14.

Carbary, J. F., T. Sotirelis, P. T. Newell, and C.-I. Meng (2003), Auroral boundary correlations between UVI and DMSP, *J. Geophys. Res.*, *108* (A1), 1018, doi:10.1029/2002JA009378.

Cowley, S. W. H. (1981a), Asymmetry effects associated with the x-component of the IMF in a magnetically open magnetosphere, *Planet. Space Sci.*, *29*, 809–818.

Cowley, S. W. H. (1981b), Magnetospheric asymmetries associated with the y-component of the IMF, *Planet. Space Sci.*, *29*, 79–96.

Cowley, S. W. H., and M. Lockwood (1992), Excitation and decay of solar wind-driven flows in the magnetosphere-ionosphere system, *Ann. Geophys.*, 103–115.

Cowley, S. W. H., J. P. Morelli, and M. Lockwood (1991), Dependence of convective flows and particle precipitation in the high-latitude dayside ionosphere on the x and y components of the interplanetary magnetic field, *J. Geophys. Res.*, *96*, 5557–5564, doi:10.1029/90JA02063.

de la Beujardiere, O., L. R. Lyons, and E. Friis-Christensen (1991), Sondrestrom radar measurement of the reconnection electric field, *J. Geophys. Res.*, *96*, 13,907–13,912, doi:10.1029/91JA01174.

Dungey, J. W. (1961), Interplanetary magnetic field and the auroral zones, *Phys. Rev. Lett.*, *6*, 47–48.

Frank, L. A., and J. B. Sigwarth (2003), Simultaneous images of the northern and southern auroras from the Polar spacecraft: An auroral substorm, *J. Geophys. Res.*, *108*(A4), 8015, doi:10.1029/2002JA009356.

Frank, L. A., J. B. Sigwarth, J. D. Craven, J. P. Cravens, J. S. Dolan, M. R. Dvorsky, P. K. Hardebeck, J. D. Harvey, and D. W. Muller (1995), The visible imaging system VIS for the Polar spacecraft, *Space Sci. Rev.*, *71*, 297–328.

Frey, H. U., S. B. Mende, H. B. Vo, M. Brittnacher, and G. K. Parks (1999), Conjugate observation of optical aurora with polar satellite and ground-based cameras, *Adv. Space Res.*, *23*, 1647–1652.

Haaland, S. E., G. Paschmann, M. Forster, J. M. Quinn, R. B. Torbert, C. E. McIlwain, H. Vaith, P. A. Puhl-Quinn, and C. A. Kletzing (2007), High-latitude plasma convection from cluster EDI measurements: method and IMF-dependence, *Ann. Geophys.*, *25*, 239–253.

Hubert, B., S. E. Milan, A. Grocott, C. Blockx, S. W. H. Cowley, and J.-C. Gérard (2006), Dayside and nightside reconnection rates inferred from IMAGE-FUV and Super Dual Auroral Radar Network data, *J. Geophys. Res.*, *111*, A03217, doi:10.1029/2005JA011140.

Hubert, B., S. E. Milan, A. Grocott, S. W. H. Cowley, and J. C. Gerard (2008), Open magnetic flux and magnetic flux closure during sawtooth events, *Geophys. Res. Lett.*, *35*, L23301, doi:10.1029/2008GL036374.

Jørgensen, T. S., E. Friis-Christensen, and J. Wilhjelm (1972), Interplanetary magnetic-field directions and high-latitude ionospheric currents, *J. Geophys. Res.*, *77*, 1976–1977.

Lam, M. M., M. Pinnoch, and E. F. Donovan (2006), Observations of nightside magnetic reconnection during substorm growth and expansion phases, *J. Geophys. Res.*, *111*, A05209, doi:10.1029/2005JA011356.

Laundal, K. M., and N. Østgaard (2009), Asymmetric auroral intensities in the Earth's Northern and Southern Hemispheres, *Nature*, *460*, 491–493.

Liou, K., P. T. Newell, D. G. Sibeck, C.-I. Meng, M. Brittnacher, and G. Parks (2001), Observation of imf and seasonal effects in the location of auroral substorm onset, *J. Geophys. Res.*, *106*, 5799–5810, doi:10.1029/2000JA003001.

Lockwood, M., S. W. H. Cowley, and M. P. Freeman (1990), The excitation of plasma convection in the high-latitude ionosphere, *J. Geophys. Res.*, *95*, 7961–7972, doi:10.1029/JA095iA06p07961.

Mende, S. B., H. U. Frey, T. J. Immel, J.-C. Gérard, B. Hubert, and S. A. Fuselier (2003a), Global imaging of proton and electron aurorae in the far ultraviolet, *Space Sci. Rev.*, *109*, 211–254.

Mende, S. B., H. U. Frey, B. J. Morsony, and T. J. Immel (2003b), Statistical behavior of proton and electron auroras during substorms, *J. Geophys. Res.*, *108*(A9), 1339, doi:10.1029/2002JA009751.

Mende, S. B., et al. (2000), Far ultraviolet imaging from the IMAGE spacecraft. 2. wideband FUV imaging, *Space Sci. Rev.*, *91*, 271–285.

Milan, S. E., M. Lester, S. W. H. Cowley, K. Oksavik, M. Brittnacher, R. A. Greenwald, G. Sofko, and J.-P. Villain (2003), Variations in the polar cap area during two substorm cycles, *Ann. Geophys.*, *21*, 1121–1140.

Milan, S. E., G. Provan, and B. Hubert (2007), Magnetic flux transport in the dungey cycle: A survey of dayside and nightside reconnection rates, *J. Geophys. Res.*, *112*, A01209, doi:10.1029/2006JA011642.

Milan, S. E., P. D. Boakes, and B. Hubert (2008), Response of the expanding/contracting polar cap to weak and strong solar wind driving: Implications for substorm onset, *J. Geophys. Res.*, *113*, A09215, doi:10.1029/2008JA013340.

Milan, S. E., A. Grocott, C. Forsyth, S. M. Imber, P. D. Boakes, and B. Hubert (2009), A superposed epoch analysis of auroral evolution during substorm growth, onset and recovery: open magnetic flux control of substorm intensity, *Ann. Geophys.*, *27*, 659–668.

Newell, P. T., C.-I. Meng, and K. M. Lyons (1996), Suppression of discrete aurorae by sunlight, *Nature*, *381*, 766–767.

Østgaard, N., S. B. Mende, H. U. Frey, T. J. Immel, L. A. Frank, J. B. Sigwarth, and T. J. Stubbs (2004), Interplanetary magnetic field control of the location substorm onset and auroral features in the conjugate hemisphere, *J. Geophys. Res.*, *109*, A07204, doi:10.1029/2003JA010370.

Østgaard, N., J. Moen, S. B. Mende, H. U. Frey, T. J. Immel, P. Gallop, K. Oksavik, and M. Fujimoto (2005a), Estimates of magnetotail reconnecton rate based on IMAGE FUV and EISCAT measurements, *Ann. Geophys.*, *23*, 123–134.

Østgaard, N., N. A. Tsyganenko, S. B. Mende, H. U. Frey, T. J. Immel, M. Fillingim, L. A. Frank, and J. B. Sigwarth (2005b), Observations and model predictions of substorm auroral asymmetries in the conjugate hemispheres, *Geophys. Res. Lett.*, *32*, L05111, doi:10.1029/2004GL022166.

Østgaard, N., S. B. M. abd, H. U. Frey, J. B. Sigwarth, A. Aasnes, and J. Weygand (2007), Auroral conjugacy studies based on global imaging, *J. Atmos. Terr. Phys.*, *69*, 249–255.

Oznovich, I., R. W. Eastes, R. E. Hoffman, M. Tur, and I. Glaser (1993), The aurora at quiet magnetospheric conditions: Repeatability and dipole tilt angle dependence, *J. Geophys. Res.*, *98*, 3789–3797, doi:10.1029/92JA01950.

Parker, E. N. (1996), The alternative paradigm for magnetospheric physics, *J. Geophys. Res.*, *105*, 10,587–10,625, doi:10.1029/95JA02866.

Provan, G., M. Lester, S. B. Mende, and S. E. Milan (2004), Statistical study of high-latitude plasma flow during magnetospheric substorms, *Ann. Geophys.*, *22*, 3607–3624.

Richmond, A. D. (1995), Ionospheric electrodynamics using magnetic apex coordinates, *J. Geomagn. Geoelectr.*, *47*, 191–212.

Ruohoniemi, J. M., and R. A. Greenwald (2005), Dependencies of high-latitude plasma convection: Consideration of interplanetary magnetic field, seasonal, and universal time factors in statistical patterns, *J. Geophys. Res.*, *110*, A09204, doi:10.1029/2004JA010815.

Sato, N., A. Kadokura, Y. Ebihara, H. Deguchi, and T. Saemundsson (2005), Tracing geomagnetic conjugate points using exceptionally similar synchronous auroras, *Geophys. Res. Lett.*, *32*, L17109, doi:10.1029/2005GL023710.

Siscoe, G. L., and T. S. Huang (1985), Polar cap inflation and deflation, *J. Geophys. Res.*, *90*, 543–547.

Stenbaek-Nielsen, H. C., and A. Otto (1997), Conjugate auroras and the interplanetary magnetic field, *J. Geophys. Res.*, *102*, 2223–2232, doi:10.1029/96JA03563.

Stubbs, T. J., R. R. Vondrak, N. Østgaard, J. B. Sigwarth, and L. A. Frank (2005), Simultaneous observations of the auroral ovals in both hemispheres under varying conditions, *Geophys. Res. Lett.*, *32*, L03103, doi:10.1029/2004GL021199.

Vasyliunas, V. M. (1984), Steady state aspects of magnetic field line merging, in *Magnetic Reconnection in Space and Laboratory Plasmas*, *Geophys. Mongr. Ser.*, vol. 30, edited by E. Hones Jr., pp. 25–31, AGU, Washington D. C.

Vasyliunas, V. M. (2005), Relation between magnetic fields and electric currents in plasmas, *Ann. Geophys.*, *23*, 2589–2597.

Vorobyev, V. G., O. I. Yagodkina, D. Sibeck, K. Liou, and C.-I. Meng (2001), Aurora conjugacy during substorms: Coordinated antarctic ground and polar ultraviolet observations, *J. Geophys. Res.*, *106*, 24,579–24,591, doi:10.1029/2001JA900025.

Wing, S., P. T. Newell, D. G. Sibeck, and K. B. Baker (1995), A large statistical study of the entry of interplanetary magnetic field y-component into the magnetosphere, *Geophys. Res. Lett.*, *22*, 2083–2086, doi:10.1029/95GL02261.

H. Frey, Space Sciences Laboratory, University of California, 7 Gauss Way, Berkeley, CA 94720-7450, USA. (hfrey@ssl.berkeley.edu)

K. M. Laundal and N. Østgaard, Department of Physics and Technology, University of Bergen, Allegt. 55, N-5007 Bergen, Norway. (karl.laundal@ift.uib.no; nikolai.ostgaard@ift.uib.no)

K. Snekvik, Finnish Meteorological Institute, PO Box 503, FIN-00101 Helsinki, Finland. (kristian.snekvik@fmi.fi)